Proceedings of the

11th WORKSHOP ON TWO-PHASE FLOW PREDICTIONS

Merseburg, April 5 - 8, 2005

Edited by:

M. Sommerfeld

Lehrstuhl für Mechanische Verfahrenstechnik

Institut für Verfahrenstechnik

Fachbereich Ingenieurwissenschaften

Martin-Luther-Universität Halle-Wittenberg

06099 Halle (Saale), Germany

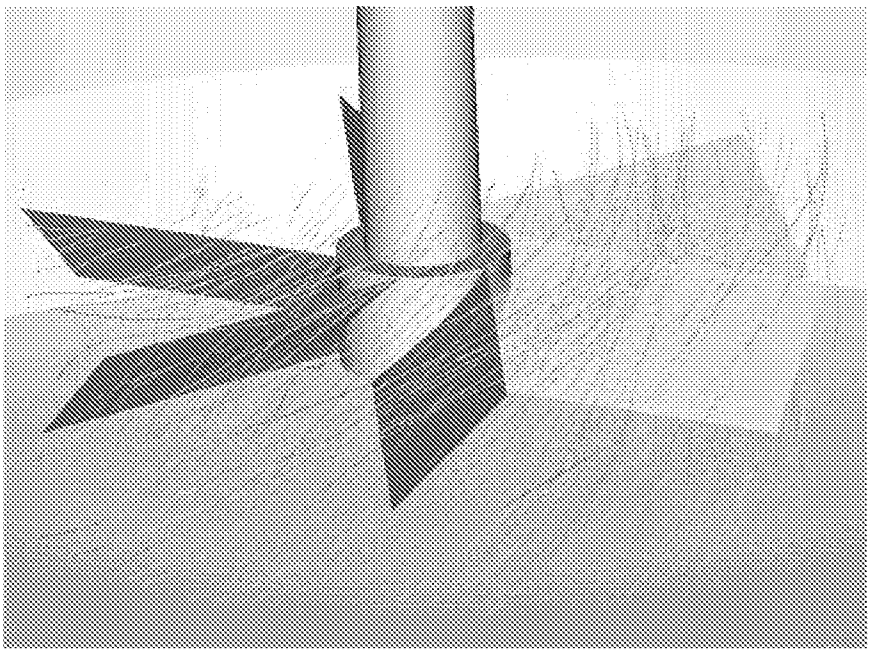

Particle motion around a pitched blade impeller

The Workshop is co-sponsored by:

ERCOFTAC (European Research Community on Flow, Turbulence and Combustion)

Deutsche Forschungsgemeinschaft

Die Deutsche Bibliothek - CIP-Einheitsaufnahme

Workshop on Two-Phase Flow Predictions <11, 2005, Merseburg>:

Proceedings of the 11th Workshop on Two-Phase Flow Predictions: Merseburg, April 5 - 8, 2005 / ed. by: M. Sommerfeld,

Lehrstuhl für Mechanische Verfahrenstechnik, Institut für Verfahrenstechnik, Fachbereich Ingenieurwissenschaften, Martin-Luther-Universität Halle-Wittenberg. - Halle (Saale): Univ., 2005

ISBN 3-86010-767-4

0101 deutsche buecherei

Derivation of closures for single air bubbles in water using an improved 3D Front Tracking model

W. Dijkhuizen, M. van Sint Annaland[1], J.A.M. Kuipers

Chemical Reaction Engineering group, University of Twente.
[1] Corresponding author: tel. +31-53-4894478; fax +31-53-4892882.
P.O. Box 217, 7500 AE Enschede, The Netherlands.
E-mail address: M.vanSintAnnaland@utwente.nl

Abstract

Using a 3D Front Tracking (FT) model, closures for the drag, lift and virtual mass forces have been derived for single freely deformable air bubbles rising in water. The combination of a large surface tension force, a high density ratio as well as a high Reynolds number poses a severe numerical challenge for Direct Numerical Simulations. Therefore, the numerical implementation of the FT model was improved to allow simulation of very small air bubbles (~1 mm) in water using realistic physical properties without numerical problems or unphysical volume changes. The computed drag force coefficients for air bubbles in the range of 1-5 mm compare reasonably well with experimental data from literature. The small discrepancies may be explained by the extremely high sensitivity of the air/water system for surface contaminants, as has been extensively reported in the literature. For an initially spherical air bubble in initially quiescent water a virtual mass coefficient of 0.53 was computed for all diameters air bubbles, which compares very well with the theoretical result of 0.50. The simulated coefficient converges to the theoretical value when the grid is further refined. Finally, a lift force coefficient of 0.5 was found for a 4 mm air bubble rising in a linear shear flow, which is somewhat higher than experimental data reported in the literature for lower Reynolds numbers.

Introduction

Multiphase gas/liquid and gas/liquid/liquid flows are widely encountered, in natural phenomena as well as in (chemical) industry. The large scale of the industrial equipment contrasts sharply with the small scale of bubbles and droplets. Because of this difference in scales, it is virtually impossible to capture all the details of the flow field with the currently available computational resources in a single model. To overcome this problem a successful description of multi-phase flows therefore has to be based on a sound multi-level modelling approach (van Sint Annaland et al., 2003), which is schematically indicated in Fig. 1.

Direct Numerical Simulations (DNS) are used at the smallest time and length scales to study the behaviour of a single or a few gas bubbles or liquid droplets. Combined with feedback from dedicated experiments, these models can be used to derive closure equations for the interaction between the dispersed phase and the main liquid, which can then be used in higher level models. One step higher, the Euler-Lagrange or bubble tracking model can be used to study the interactions between large numbers of bubbles and the impact on the macroscopic flow structures. Each dispersed element in this model is treated as a discrete element and the forces acting on it are computed from the closure equations. Because of this discrete approach a large number of bubbles (~100,000) can be simulated with acceptable computation time. However, in industrial applications multi-phase flows with even a much higher number of dispersed elements are encountered, which

requires a continuum approach. At this highest level of modelling the Euler-Euler or multi-fluid continuum models, bubbles lose their discrete identity, which enables the simulation of very large systems and study large-scale heterogeneous structures in the flow.

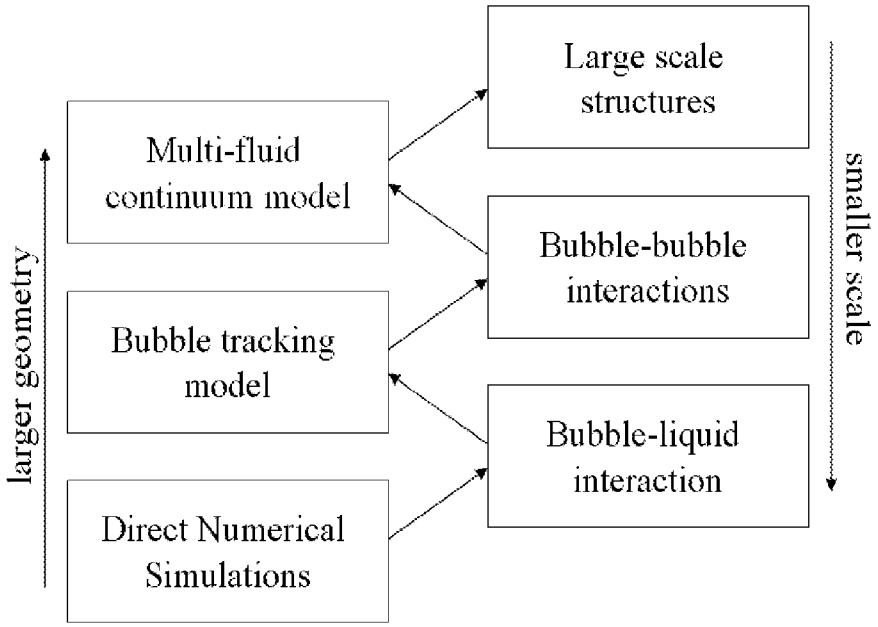

Figure 1: Schematic overview of a Multi-level modeling approach applied to gas-liquid flows.

Accurately describing the behaviour of gas-liquid systems with the higher level models has proven difficult, because detailed knowledge on the behaviour of single bubbles or droplets in complex flow fields is lacking. For example, even the behaviour of a single air bubble rising in quiescent water is not yet completely understood: not only physical properties like the density, viscosity and surface tension affect the behaviour of the bubbles, but also the presence of small amounts of surface active impurities (Grace et al., 1976). More recently, Wu and Gharib (2002) and Tomiyama et al. (2002a) independently pointed out that the initial shape of the bubble can affect its terminal rise velocity. This illustrates the intrinsic complexities in performing dedicated experiments.

Problems arise in the description of the motion of a single bubble from the complex interaction between the bubble shape dynamics and the flow field in its vicinity. This is particularly difficult at high Reynolds numbers, which are encountered in the industrially important case of dispersed air bubbles in water. With the advances that have been made in CFD during the last decade, now the shape and interface dynamics can be studied in great detail. In this study a DNS has been used to study the behaviour of air bubbles rising in water.

When it comes to DNS several models have been proposed and used in the literature, where it is important to realise that every model has its own strong and weak points (van Sint Annaland et al., 2005a). By far the most popular model is the Volume Of Fluid (VOF) model, which typically involves reconstruction of the interface using the spatial distribution of the volume fraction of the phases. The major advantage of this model is that it is relatively easy to implement and the volume of the dispersed elements is very well conserved. However, these advantages come at a high cost: the interface is not explicitly tracked, but has to be reconstructed from the phase fractions. First of all this causes problems when calculating the surface tension force, which is a singular force acting on the interface. Secondly, a poor interface reconstruction combined with a large density ratio may cause the numerical method to become unstable. Also parasitic currents in the vicinity of the

interface may develop. These drawbacks of the VOF method are especially limiting for small air bubbles (~ 1 mm) in water, where a high density ratio and a high surface tension force are combined.

In this work a full 3D Front Tracking (FT) model is used, following the work of Unverdi and Tryggvason (1992). The advantage of this model is that the interface is explicitly tracked by interconnected points which form triangular markers. In sharp contrast with VOF this makes it possible to describe the shape and location of the interface with a very high accuracy. The first benefit is that the accuracy of the surface tension force calculation can be improved (Popinet and Zaleski, 1998). Secondly because there is no interface reconstruction, parasitic currents are greatly reduced. However, this comes at a price: the volume of the dispersed phases is not intrinsically conserved and because of deformation, marker points have to be periodically added and removed (surface remeshing). For a detailed comparison of different DNS methods the interested reader is referred to Scardovelli and Zaleski (1999).

3D Front Tracking was used in this work to calculate the drag, virtual mass and lift forces directly, without the need for any kind of closures. The results of the numerical simulations are compared with experimental data. In all of our simulations realistic physical properties were used, for instance a density ratio of 800 for air bubbles in water. Before this was possible, some modifications had to be made to the original model, in order to improve mass conservation for small air bubbles in water. These modifications were extensively verified using standard test cases as reported by van Sint Annaland et al. (2005b).

Front tracking model

In the FT model the Navier-Stokes equations are solved together with the continuity equation for incompressible media:

$$\nabla \cdot \mathbf{u} = 0 \tag{1}$$

$$\frac{\partial}{\partial t}(\rho \mathbf{u}) + \nabla \cdot \rho \mathbf{u}\mathbf{u} = -\nabla p + \rho \mathbf{g} + \nabla \cdot \mu \left[(\nabla \mathbf{u}) + (\nabla \mathbf{u})^T \right] + \mathbf{F}_\sigma \tag{2}$$

where the density ρ and the viscosity μ are locally averaged over all the phases present, based on the phase fraction F_i. The surface tension force is included as a volumetric force $\mathbf{F}_\sigma$ acting only in the vicinity of the interface.

The Navier-Stokes equations are solved on a staggered Cartesian mesh with a finite volume technique using an implicit treatment of the pressure gradient and an explicit treatment of the convection and diffusion terms. For the convection term a second order flux delimited Barton scheme (Centrella and Wilson, 1984) and for the diffusion term a standard second order finite difference scheme is used. To be able to simulate large density ratios, the Navier-Stokes equations are rewritten in their non-conservative form using the continuity equation (Van Sint Annaland et al., 2003):

$$\rho \left[\frac{\partial \mathbf{u}}{\partial t} + \nabla \cdot \mathbf{u}\mathbf{u} \right] = -\nabla p + \rho \mathbf{g} + \nabla \cdot \mu \left[(\nabla \mathbf{u}) + (\nabla \mathbf{u})^T \right] + \mathbf{F}_\sigma \tag{3}$$

A two step projection-correction method is then used to solve the two equations: first the velocity is calculated using all the explicit terms in the Navier-Stokes equations and secondly a robust ICCG

method is used to calculate the pressure correction to satisfy the incompressibility constraint. A higher order discretisation scheme was applied for the divergence operator based on the work of Peskin and Printz (1993).

Average fluid properties

For the local density linear weighing of all the phase fractions is used:

$$\rho = \sum_{i=1}^{nphases} F_i \rho_i \tag{4}$$

where F_i represents the fraction of phase i. Usually the viscosity is also linearly averaged, but here a more fundamental approach is used based on harmonic averaging of the kinematic viscosities (Prosperetti, 2001):

$$\frac{\rho}{\mu} = \sum_{i=1}^{nphases} F_i \frac{\rho_i}{\mu_i} \tag{5}$$

Surface tension

Making direct use of the triangulation of the interface, the surface tension force acting on a triangular marker m is calculated by taking a contour integral along its edges (see Fig. 2):

$$\mathbf{F}_{\sigma,m} = \frac{\sigma}{\Delta x \Delta y \Delta z} \oint_l (\mathbf{t}_m \times \mathbf{n}_m) dl \tag{6}$$

where $\mathbf{t}_m$ is the counter clockwise unit tangent vector along the edges of the marker m and l is the length of these tangent vectors (the perimeter of the marker).

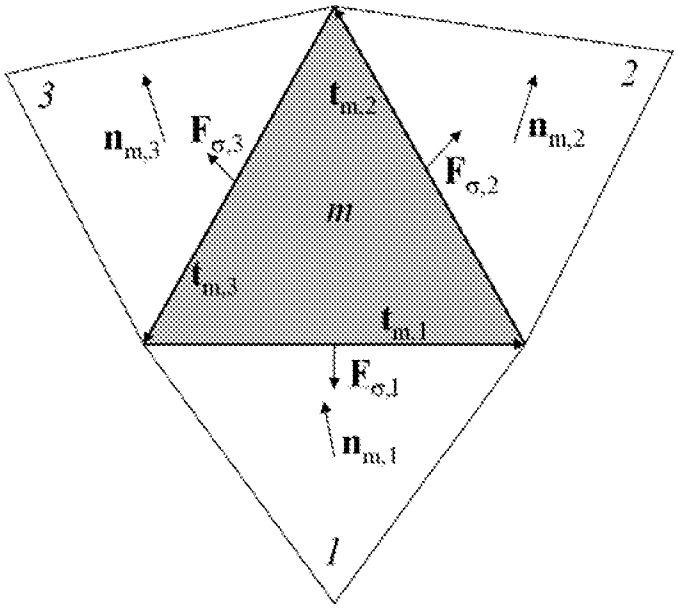

Figure 2: Schematic illustration of the direct surface tension force calculation.

This method avoids the computation of the numerically inaccurate curvature and can be used for surfaces with a very high curvature with less numerical instability and better accuracy (Gunsing, 2004). The surface tension force is mapped on to the Eulerian grid using a summation over all the markers m and their edges l:

$$\mathbf{F}_\sigma = \frac{\sum_m \sum_l D\left(\mathbf{x} - \mathbf{x}_{m,l}\right)\sigma\left(\mathbf{t}_{m,l} \times \mathbf{n}_{m,l}\right)}{\Delta x \Delta y \Delta z} \tag{7}$$

where $\mathbf{t}_{m,l}$ is the tangential vector and D is the distribution kernel, for which in this work density weighing (Deen et al., 2004) is used. Density weighing avoids mapping of the surface tension force to a cell with a low mass, which can cause large distortions of the velocity field near the interface. Tryggvason et al. (2001) use a polynomial fit to obtain the normal and tangential vectors, but with our method the surface tension force is calculated directly from the discrete triangulation.

Calculation of the phase fractions

In the FT model the phase fractions are calculated by a method proposed by Unverdi and Tryggvason (1992):

$$\begin{aligned} \nabla^2 F &= \nabla \cdot \mathbf{G} \\ \mathbf{G} &= \sum_m D\left(\mathbf{x} - \mathbf{x}_m\right)\mathbf{n}_m \Delta s_m \end{aligned} \tag{8}$$

where $\mathbf{n}_m$ is the outwards pointing normal and Δs_m is the surface of the marker. First the gradient $\mathbf{G}$ is calculated from the interface markers, after which an ICCG method is used to solve this Poisson equation.

Updating the interface

Once the flow field has been found on the Eulerian grid, each marker point of the interface triangulation is moved with the local flow field. After some time the surface grid will become deformed. Some markers will become too large or too stretched, while others become too small. To maintain an adequate resolution, points will have to be added at some places and removed at other places. In this work a similar approach as described by Unverdi and Tryggvason (1992) is followed.

Derivation of the interface forces

In order to provide closures for discrete elements models, where the bubbles or droplets are considered to be spherical, the drag, virtual mass and lift coefficients are also derived assuming spherical entities. The effects of the shape of the bubble are thus implicitly lumped in the coefficients.

Drag force

Both the drag and virtual mass forces can be obtained from a simulation where initially the fluid is at rest and the bubble or droplet is released as a perfect sphere.

The drag force coefficient C_D can be computed from the terminal rise velocity of the dispersed element via a simple stationary force balance in the z-direction:

$$C_D = \frac{4}{3}\frac{\left(\rho_l - \rho_g\right)|\mathbf{g}|d_e}{\rho_l|\mathbf{w}_b|w_{b,z}} \tag{9}$$

where w_b is the bubble rise velocity and d_e its equivalent sphere diameter.

Virtual mass force

Virtual or added mass is the additional mass that has to be accelerated apart from the dispersed element itself, caused by the fact that the surrounding liquid has to be moved away from the bubble to let it rise. For a perfect sphere the analytical value is ½ (Lamb, 1932), meaning that the equivalent of half the bubble volume of liquid is added to the mass of the dispersed element when it accelerates.

The virtual mass force coefficient C_{VM} can be computed from an instationary force balance in the z-direction, yielding the following expression:

$$C_{VM} = -\frac{\rho_g}{\rho_l} + \frac{\left(\rho_l - \rho_g\right)|\mathbf{g}|}{\rho_l \dfrac{dw_{b,z}}{dt}} \tag{10}$$

It can be seen that for low pressure gas bubbles ($\rho_l >> \rho_g$) this equation reduces to eq. 11, which shows that a spherical bubble is expected to accelerate with twice the gravity constant.

$$C_{VM} = \frac{|\mathbf{g}|}{\dfrac{dw_{b,z}}{dt}} \tag{11}$$

Lift force

When a linear shear field is applied to a small dispersed element it will move towards the lower velocity, while larger bubbles or droplets will move towards the higher velocity. Tomiyama et al. (2002b) found experimentally for different viscous systems ($M>10^{-5.5}$) that this transition occurs at an Eötvos number of 6.

Finally the lift force coefficient C_L can be found by combining force balances in the direction of the velocity gradient (x-direction) and the vertical direction.

$$C_L = \frac{\dfrac{\rho_l - \rho_g}{\rho_l}|\mathbf{g}|\left(\mathbf{w}_{b,z} - u_{l,z}\right)}{\left|\mathbf{w}_b - \mathbf{u}_l\right|^2 \dfrac{du_{l,z}}{dx}} \tag{12}$$

where $\mathbf{u}_l$ is the velocity of the liquid phase.

Simulation settings

All of the simulations for the air-water system were carried out on an 80x80x80 grid with the bubble positioned at 2/3 height in the centre of the box. The initially spherical bubble was 20 Eulerian cells in diameter. A moving window concept was used for all the simulations to ensure that no computational power is wasted and the bubble is always at approximately the same distance from the walls. Finally, free-slip boundaries are used for all the walls.

Absence of grid dependency was verified by running simulations at a lower resolution (40x40x40 grid). The same values were found for the steady rise velocities of the bubbles, indicating that the drag force is relatively undemanding with respect to the detail of the flow field.

With the improvements in the numerical implementation of the FT model, it was possible to simulate very small bubbles (~1 mm diameter) using realistic properties at a temperature of 25°C and a pressure of 1.0 bar (Table 1). This was achieved without numerical instabilities or significant volume changes resulting from the treatment of the surface tension. According to the authors this is the first time that this is reported in the literature.

Table 1: Physical properties of air and water that have been used in the simulations.

Phase	Viscosity [$kg \cdot m^{-1} \cdot s^{-1}$]	Density [$kg \cdot m^{-3}$]	Surface tension [$N \cdot m^{-1}$]
Water	$1.0 \cdot 10^{-3}$	1000	0.073
Air	$1.8 \cdot 10^{-5}$	1.25	-

Drag force results

Each of the air bubbles in water was initially spherical and the fluid is at rest. This is important, because the bubbles are not forced into any kind of shape, which is known to be an important problem in experiments (Tomiyama, 2004; Wu and Gharib, 2002). The evolution of the vertical rise velocities of the bubbles in time are given in Fig. 3. It can be seen that initially bubbles rise with the same velocity and after some time they take their final value. Bubbles larger than 2 mm oscillate in a sinusoidal fashion, of which the amplitude increases with bubble size. This effect is caused by a combination of the high Reynolds number (~1000) and a small surface tension force. Larger bubbles have been successfully simulated, but the wobbling motion of these bubbles becomes highly irregular. In reality these bubbles probably break-up, which is confirmed by an absence of measurements for bubbles larger than 5 mm. However break-up is not implemented in the FT model and therefore these results have been omitted.

As noted in the introduction, the FT model has the advantage of an explicit tracking of the bubble interface. This allows us to visualise the bubble interface directly, without any form of processing whatsoever (Fig. 4). It can be seen that only the 1 mm bubble is almost spherical and for larger bubbles the shape evolves from ellipsoidal (2 mm) to more irregular shapes. The 4 and 5 mm bubbles show a continuous shape change.

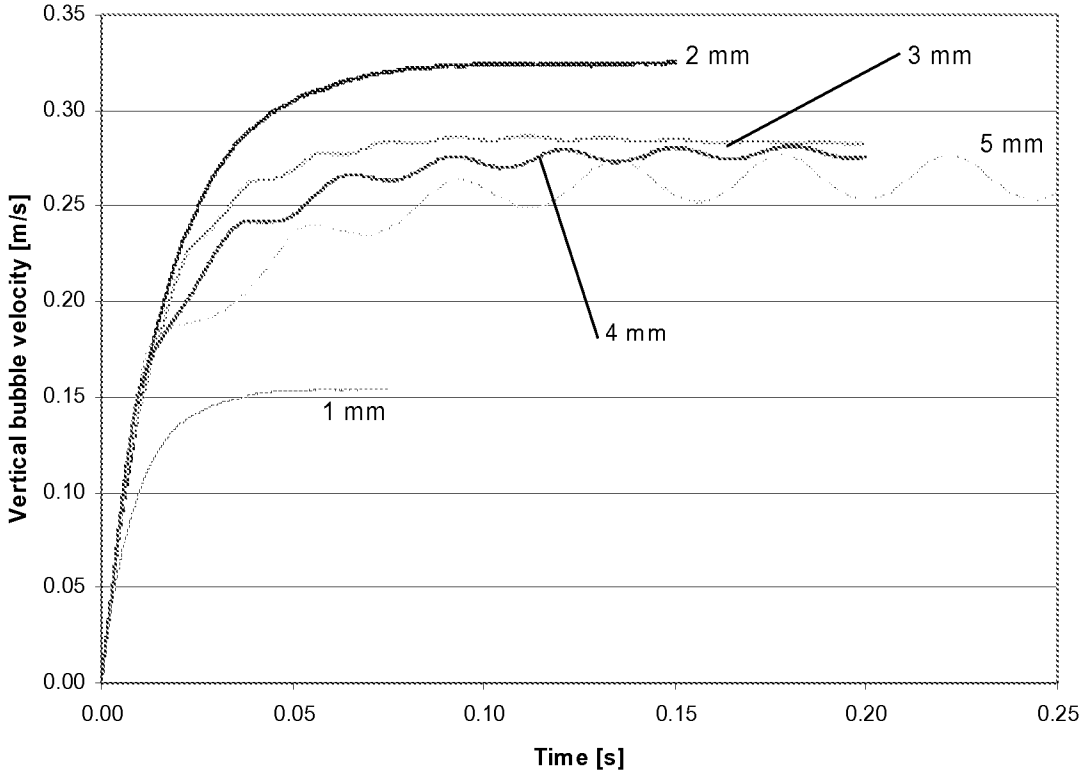

Figure 3: Simulated rise velocities as a function of time for different sizes of air bubbles in water.

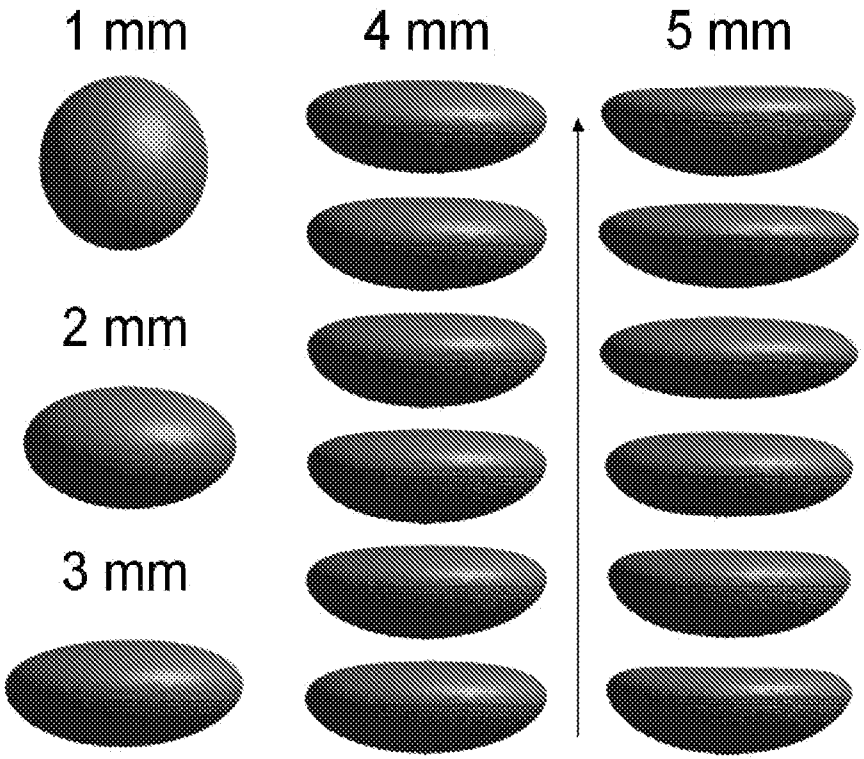

Figure 4: Bubble interface for different air bubbles rising in water, as calculated by the 3D FT model. The 4 and 5 mm bubbles continuously change shape in wobbling motion.

Finally the drag force coefficient can be computed from the terminal rise velocities of the bubbles. This allows for a detailed comparison with different experimental relations reported in the literature (Fig. 5). It can be seen that there is some discrepancy between the simulation results and the different experimental relations from literature, especially for small bubbles (1-2 mm). Overall the simulations agree reasonably well with the experimental correlations.

Grace et al. (1976) published a relation for the drag force on a bubble or droplet, based on measurements in contaminated liquids from many different sources. There is also a relation (actually a correction) available for pure systems, but due to the large scatter in the experimental data it is omitted here.

Tomiyama (1998) has derived a drag law for both contaminated as well as pure liquids. It is based on a combination of existing relations and relations obtained from potential flow theory for a bubble in an infinite liquid. This model has been validated by a large number of measurements for air bubbles in distilled water (Tomiyama, 2004). During these measurements it was found that the initial shape deformation during injection of the bubbles influenced the terminal rise velocity of the bubbles to such an extent that the measurements are scattered throughout the area between the lines in Fig. 5. This effect was separately confirmed by Wu and Gharib (2002).

Duineveld (1994) has performed measurements in ultrapurified water with a very gentle injection method, which compares best with the ideal initial condition and absence of surface active contaminants assumed in the simulations. The range of Reynolds numbers above 450 is particularly interesting, because it shows us that surface active impurities slow down the bubbles. The FT result for a 2 mm air bubble agrees very well with the experimental results by Duineveld, but unfortunately his measurements are limited to a bubble diameter of 0.7 to 2.0 mm. In the near future more simulations will be performed in this range for a more detailed comparison.

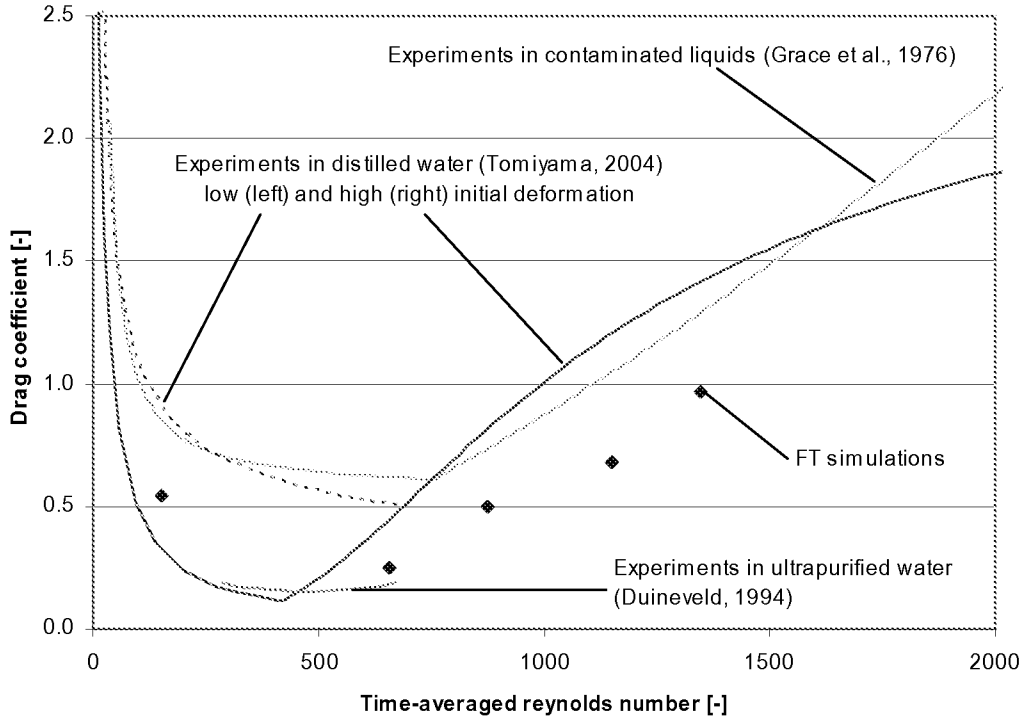

Figure 5: Comparison of the drag force coefficient for air bubbles rising in quiescent water for both experiments from literature and 3D FT simulations performed in this work.

Virtual mass force results

According to potential flow theory the theoretical value of the virtual mass coefficient for a spherical object is 0.5. Mouguin and Magnaudet (2002) have shown that this value can also be used for a spherical bubble in a viscous flow.

From the same simulations that were done for the drag force, a virtual mass coefficient of 0.53 was found for all sizes of spherical bubbles. The agreement with literature is quite good, especially considering that the bubble spans only about 20 grid cells. A detailed analysis of the grid-dependency showed us that the virtual mass coefficient indeed converges to the analytical value of 0.50 for very fine grids (0.52 for a 100^3 grid).

Lift force results

In order to complete the set of closures for an air-water system, the lift force has to be studied. This force only acts when a velocity gradient is present perpendicular to the direction of movement. The easiest and most well defined experiment imaginable is to let an air bubble rise in a linear shear field. Due to the wobbling nature of air bubbles in water, simulations times in the order of 3 seconds will be necessary to average out the zigzagging motion of the bubbles. However these simulations are very time-consuming and up till now only 0.5 seconds of a 4 mm air bubble in water have been simulated. The shear stress used was equal to 5 s^{-1}. Figure 6 shows the evolution of the bubble shape in time for 1.5 cycles of the stationary situation. It can be seen that the shape changes are very significant, but the FT model is always capable of describing the interface with sufficient detail.

In Fig. 7 the position of the bubble is plotted as a function of time. It can be seen that the bubble quickly attains its terminal rise velocity, but its perpendicular movement takes more time to get stationary. After about 0.25 seconds, the zigzagging motion of the bubble does become stationary and the bubble slowly starts to move to the side with the highest velocity. A time-averaged lift force coefficient of 0.5 was found, which is higher than the experimental value of 0.3 by Tomiyama et al. (2002b). However it should be noted that his measurements were carried out at a Morton number larger than $10^{-5.5}$. This means that the experimental bubbles have a much more stable shape and consequently do not meander through the column. The impact of the zigzagging motion of the air bubbles on the lift force is still unclear and will be investigated in the near future. Moreover simulations will be carried out for longer simulation times and for different bubble diameters and shear rates.

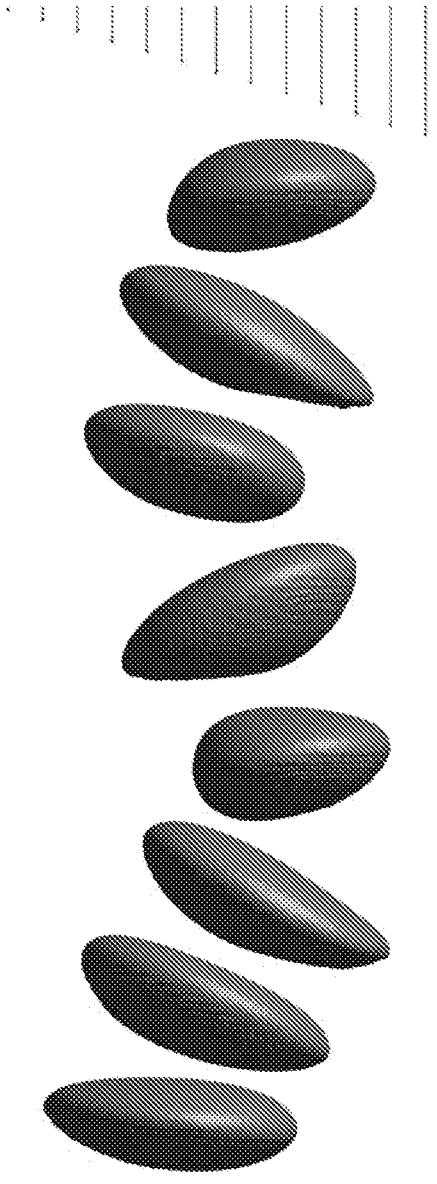

Figure 6: consecutive images of the interface of a 4 mm air bubble rising in a linear shear field.

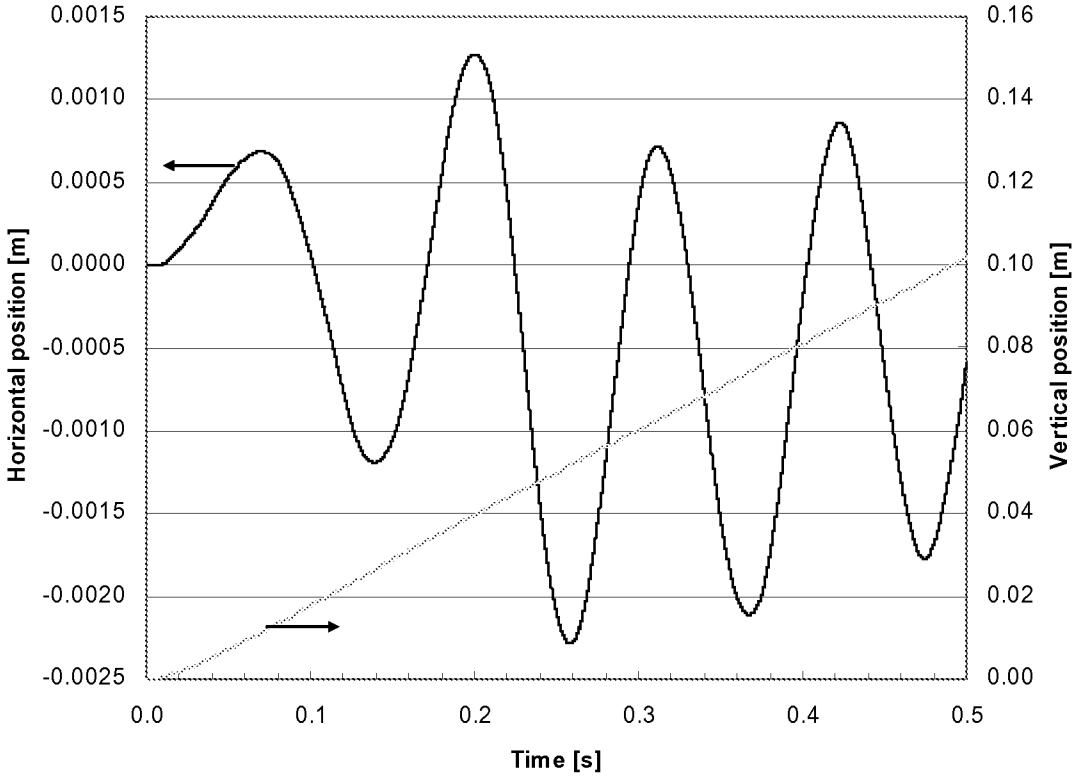

Figure 7: bubble position as a function of time for a 4 mm air bubble in a linear shear field.

Conclusions

A 3D FT model was developed and successfully used to investigate closures for interface forces acting on air bubbles in pure water. Improvements were made to the model, in order to be able to simulate small air bubbles (~1 mm) using realistic physical properties without numerical problems or unacceptable volume changes. According to the authors' knowledge this is the first time that this has been reported in the literature.

The computed drag force coefficient for air bubbles with an equivalent sphere diameter of 1 to 5 mm compare well with experimentally obtained results for ultra pure water. Virtual mass force coefficients of 0.53 were found for spherical air bubbles with a diameter between 1 and 5 mm using an 80x80x80 grid. With an even higher grid resolution the virtual mass coefficient converges to the theoretical value of 0.50. A lift force coefficient of 0.5 was found for a 4 mm air bubble in water in a linear shear field with a shear of 5 s^{-1}. This value is somewhat higher than was found experimentally (0.3). However, these experiments were carried out at significantly lower Reynolds numbers. In the future longer simulations will be run for different bubble sizes and shear rates. Also, the impact of the meandering motion of an air bubble on the lift force will be investigated.

Acknowledgement

This work is part of the research programme of the Stichting voor Fundamenteel Onderzoek der Materie (FOM), financially supported by the Nederlandse Organisatie voor Wetenschappelijk Onderzoek (NWO) and Shell Global Solutions.

References

Centrella, J., Wilson, J., 1984: Planar Numerical Cosmology, II, The difference equations and numerical tests; Astrophysical J. Supplement Series, **54**, 229-249.

Deen, N.G., van Sint Annaland, M., Kuipers, J.A.M., 2004: Multi-scale Modeling of Dispersed Gas-Liquid Two-Phase Flow; Chem. Eng. Sci., **59**, 1853-1861.

Duineveld, P.C., 1994: Bouncing and coalescence of two bubbles in water; Ph.D. thesis, University of Twente, The Netherlands.

Grace, J.R., Wairegi, T., Nguyen, T.H., 1976: Shapes and velocities of single drops and bubbles moving freely through immiscible liquids; Trans. Instn. Chem. Engrs., **54**, 116-120.

Gunsing, M., 2004: Modelling of bubbly flows using volume of fluid, front tracking and discrete bubble models; Ph.D. thesis, University of Twente, The Netherlands.

Lamb, H., 1932: Hydrodynamics; Cambridge University Press, London.

Mouguin, G., Magnaudet, J., 2002: The generalized Kirchhoff equations and their application to the interaction between a rigid body and an arbitrary time-dependant viscous flow; Int. J. Multiphase Flow, **28**, 1837-1851.

Peskin, C.S., Printz, B.F, 1993: Improved volume conservation in the computation of flows with immersed elastic boundaries; J. Comp. Phys., **105**, 33-46.

Popinet, S., Zaleski, S., 1999: A Front Tracking algorithm for the accurate representation of surface tension; Int. J. Numer. Methods Fluids, **30**, 775-794.

Prosperetti, A., 2001: Navier-Stokes numerical algorithms for free-surface flow computations: An overview; Drop Surface Interactions, **21**.

Scardovelli, R., Zaleski, S., 1999: Direct Numerical Simulation of Free Surface and Interfacial Flow; Annu. Rev. Fluid Mech., **31**, 567-603.

Tomiyama, A., 1998: Struggle with Computational Bubble Dynamics", Third Int. Conf. on Multiphase Flow, Lyon, France.

Tomiyama, A., Celata, G.P., Hosokawa, S., Yoshida, S., 2002a: Terminal velocity of single bubbles in surface tension force dominant regime; Int. J. Multiphase Flow, **28**, 1497-1519.

Tomiyama, A., Tamai, H., Zun, I., Hosokawa, S., 2002b: Transverse migration of single bubbles in simple shear flows; Chem. Eng. Sci., **57**, 1849-1858.

Tomiyama, A., 2004: Drag, lift and virtual mass forces acting on a single bubble; 3rd Int. Symp. On Two-Phase Modeling and Experimentation, Pisa, Italy, September 22-24.

Tryggvason, G., Bunner, B., Esmaeeli, A., Juric, D., Al-Rawahi, N., Tauber, W., Han, J., Nas, S., Jan, Y.J., 2001: A front tracking method for the computations of multiphase flow; J. Comp. Phys., **169**, 708-759.

Unverdi, S.O., Tryggvason, G., 1992: A front-tracking method for viscous incompressible multi-fluid flows; J. Comp. Phys., **100**, 25-37.

Van Sint Annaland, M., Deen, N.G., Kuipers, J.A.M., 2003: Multi-Level Modelling of Dispersed Gas-Liquid Two-Phase Flows; Series: Heat and Mass Transfer. Editors: M. Sommerfeld and D. Mewes, Springer-Verlag, 139-157.

Van Sint Annaland, M., Deen, N.G., Kuipers, J.A.M., 2005a: Numerical simulation of gas bubbles behaviour using a three-dimensional Volume of Fluid method; accepted for publication, Chem. Eng. Sci.

Van Sint Annaland, M., Dijkhuizen, W., Deen, N.G., Kuipers, J.A.M., 2005b: Numerical simulation of gas bubbles behaviour using a three-dimensional Front Tracking method; submitted, AIChE J.

Wu, M., Gharib, M., 2002: Experimental studies on the shape and path of small air bubbles rising in clean water; Phys. Fluids, **14**, L49-52.

List of symbols

C_D	drag force coefficient	[-]
C_L	lift force coefficient	[-]
C_{VM}	virtual mass coefficient	[-]
D	distribution function	[-]
F	phase fraction	[-]
$\mathbf{F}_\sigma$	surface tension force density	$[N \cdot m^{-3}]$
G	phase fraction gradient	[-]
g	gravity constant	$[m \cdot s^{-2}]$
M	Morton number	[-]
n	normal vector	[-]
p	pressure	$[N \cdot m^{-2}]$
Re	Reynolds number	[-]
s	surface	$[m^2]$
t	time	[s]
$\mathbf{t}_m$	tangential unit vector	[-]
$\mathbf{t}_{m,l}$	tangential vector along edge l	[m]
u	velocity	$[m \cdot s^{-1}]$
$\mathbf{u}_l$	liquid velocity	$[m \cdot s^{-1}]$
$\mathbf{w}_b$	bubble velocity	$[m \cdot s^{-1}]$
ρ	density	$[kg \cdot m^{-3}]$
μ	dynamic viscosity	$[kg \cdot m^{-1} \cdot s^{-1}]$
σ	surface tension	$[N \cdot m^{-1}]$
Δx, Δy, Δz	grid dimensions	[m]